文章编号：1001-9014(2023)06-0736-06

DOI:10.11972/j.issn.1001-9014.2023.06.005

Effects of embedded low-dimensional materials on resonant mode of distributed Bragg reflector cavity

CUI Zhuang-Zhuang[1,3,4], LIU Qing-Quan[1,2,3], XIE Mao-Bin[1,3,4], WANG Shao-Wei[1,3,4,5*], LU Wei[1,2,3,4*]

(1. State Key Laboratory of Infrared Physics, Shanghai Institute of Technical Physics, Chinese Academy of Sciences, Shanghai 200083, China;
2. School of Physical Science and Technology, ShanghaiTech University, Shanghai 201210, China;
3. Shanghai Engineering Research Center of Energy-Saving Coatings, Shanghai 200083, China;
4. University of Chinese Academy of Sciences, Beijing 100049, China;
5. Nantong Academy of Intelligent Sensing, Nantong 226000, China)

Abstract: Low-dimensional material embedded cavities have been widely used in nano-lasers and detectors etc. The effects of embedded materials on the cavity resonant mode need to be intensively studied for achieving the efficient coupling between the gain material and the cavity. The influences of embedded material thickness and position, cavity layer thickness and the number of distributed Bragg reflector pairs on the cavity resonant mode are discussed in this work. Results show that the cavity resonant mode changes periodically with different embedded positions and there is a maximum peak shift within a period of $\lambda/2$ optical path. The maximum peak shift decreases with increasing cavity thickness and is proportional to the embedded material thickness. The number of distributed Bragg reflector pairs does not affect the cavity resonant mode. These results provide guidance on the optical device design and the analysis of experimental phenomena, which can be applied to different wavelength ranges of distributed Bragg reflector cavity structures.

Key words: optical cavity, resonant mode, embedded position, distributed Bragg reflector

嵌埋材料对分布式布拉格反射镜腔共振模式的影响

崔壮壮[1,3,4], 刘清权[1,2,3], 谢茂彬[1,3,4], 王少伟[1,3,4,5*], 陆 卫[1,2,3,4*]

(1. 中国科学院上海技术物理研究所 红外物理国家重点实验室, 上海 200083;
2. 上海科技大学 物质科学与技术学院, 上海 201210;
3. 上海节能镀膜玻璃工程技术研究中心, 上海 200083;
4. 中国科学院大学, 北京 100049;
5. 南通智能感知研究院, 江苏 南通 226000)

摘要: 低维材料嵌入微腔已经广泛应用于纳米激光器和探测器等。为了实现增益材料和光学微腔之间的有效耦合, 需要深入研究嵌埋材料对腔共振模式的影响。本文主要讨论了嵌埋材料的厚度、位置、腔层厚度以及分布式布拉格反射镜的对数对腔供着模式的影响。结果表明, 腔共振模式随嵌埋材料位置的不同呈现周期性变化并且在$\lambda/2$光程周期内存在最大峰位移。最大峰位移随腔层厚度增加而减小, 但与嵌埋材料的厚度成正比。分布式布拉格反射镜的对数不影响腔共振模式。这些结果为光学器件的设计和实验现象的分析提供了指导, 并且可以应用于不同波长分布式布拉格反射腔结构。

关 键 词: 光学腔; 共振模式; 嵌埋位置; 分布式布拉格反射镜

中图分类号: TN256 **文献标识码**: A

Received date: 2023-02-02, **revised date**: 2023-03-20 **收稿日期**: 2023-02-02, **修回日期**: 2023-03-20

Foundation items: Supported by the National Key R&D Program of China (2021YFA0715500), National Natural Science Foundation of China (NSFC) (12227901) and Chinese Academy of Sciences President's International Fellowship Initiative (2021PT0007)

Biography: CUI Zhuang-Zhuang (1994-), Bozhou, Ph. D, Research area involves micro-nano devices. E-mail: cuizhuangzhuang@mail.sitp.ac.cn

*Corresponding authors: E-mail: wangshw@mail.sitp.ac.cn, luwei@mail.sitp.ac.cn

Introduction

The light-matter interaction plays a vital role in modern science and technology, which has been used in lasers, detectors, spectroscopy and so on. An optical cavity can be exploited to limit the photons at resonant wavelengths and tailor their interactions with the matter via regulated local density states. [1] Devices based on optical microcavities, such as nano-lasers[2, 3] and micro-spectrometers[4, 5], become an important part of optoelectronic research and applications. [6, 7] The optical field output of the Fabry-Perot (F-P) cavity can realize the efficient coupling with optical fiber, while the structure is simple and easy to integrate with other devices, which provides great convenience for applications. [8] Therefore, the related research based on the F-P cavity has been widely favored. An F-P cavity is composed of two parallel high reflectors, where the distributed Bragg reflector (DBR) is mainly chosen.

The rapid development of low-dimensional (LD) materials, especially two-dimensional (2D) materials has been widely used in nano-lasers and detectors due to their excellent photoelectric properties. [9-14] Nano-lasers composed of 2D materials and DBR cavities in small sizes have become an indispensable part of fully integrated nanoscale photonic and optoelectronic devices. The key to building a good laser system is to maximize the interaction between the cavity and the gain materials. However, unlike bulk materials, the thickness of 2D materials is usually only dozens of nanometers or even a single molecular layer, much thinner than the cavity layer. Therefore, the location of 2D materials is vital to the efficiency of cavity-matter coupling. In order to achieve the efficient coupling, it is necessary to study the cavity mode change and the field distribution in the cavity when embedded with 2D materials. The gain material should be aligned with the wavelength and spatial position of the cavity optical mode, to realize the accurate control of resonant wavelength of cavity mode optical field.

In the previous work, the interaction between the optical microcavity and black phosphorus was demonstrated experimentally. The stimulated emission at 3611 nm was achieved when the black phosphorus (BP) was embedded in dielectric DBR structures. And the lasing wavelength can be tuned from 3425 nm to 4068 nm by varying the thickness of BP layer. [15] The structure of a good optical microcavity, including the thickness of the cavity layer, the number of DBR pairs and the thickness of BP, is the key to realizing the above functions. And the strong coupling phenomenon has been achieved at room temperature by optimizing such a structure. [16]

In this research, the interaction between light and LD material in the DBR cavity is investigated by the transfer matrix method (TMM) systematically, with the embedded position, number of DBR pairs, cavity layer thickness and embedded material thickness. The law or trend drawn can be used to guide the design of the enhanced interaction structure between optical microcavity and LD gain materials such as BP and 2D materials, for example, by choosing the critical position of the cavity to embed.

1 Structural design and theory of calculation

Figure 1 schematically shows the 2D materials embedded in the DBR cavity. The cavity consists of the top and bottom DBRs and a cavity layer. The basic structure can be written as $(LH)^m\ xL\ E\ yL\ (HL)^m$, L and H representing the low and high refractive index materials with thicknesses of $\lambda_0/(4\times n_L)$ and $\lambda_0/(4\times n_H)$, respectively. λ_0 is the designed wavelength. E stands for embedded 2D materials. m is the number of DBR pairs. x and y control the thickness of the spacer layer. In this paper, SiO is the low n material of L and Si is the high n material of H. Black phosphorus is chosen as 2D material, which has good luminescence properties in the mid-infrared wavelength. The designed wavelength is 3.6 μm. In this calculation, the refractive indices of Si and SiO are extracted with the ellipsometry method and the absorption and dispersion of embedded materials are not considered. [17]

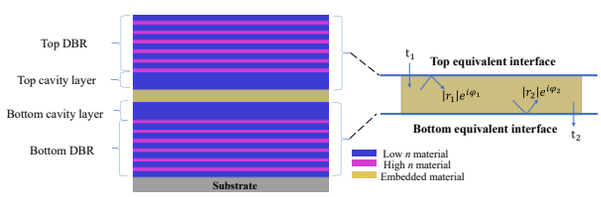

Fig. 1 The schematic diagram of the DBR cavity and its equivalent interface
图1 分布式布拉格反射镜腔的原理示意图及其等效界面示意图

Any optical multilayer can be replaced by a virtually equivalent interface, as shown on the right of Fig. 1. The top DBR and top cavity layer are equivalent to the top equivalent interface. The bottom DBR and bottom cavity layer are equivalent to the bottom equivalent interface. Without considering the influence of substrate, the media on both sides of the film are assumed to have the same admittance, so we obtain the transmittance as:

$$T = |t|^2 = \frac{|t_1 t_2|^2}{|1 - r_1 r_2 e^{-2i\delta}|^2}, \quad (1)$$

$$\text{Let, } r_1 = |r_1| e^{i\varphi_1}, r_2 = |r_2| e^{i\varphi_2}, \quad (2)$$

$$\text{So, } T = \frac{|t_1 t_2|^2}{|1 - |r_1||r_2| e^{i(\varphi_1 + \varphi_2 - 2\delta)}|^2}, \quad (3)$$

$$= \frac{|t_1 t_2|^2}{(1 - |r_1||r_2|)^2} \cdot \frac{1}{1 + (1 - |r_1||r_2|)^2 \cdot sin^2 \frac{1}{2}(\varphi_1 + \varphi_2 - 2\delta)}, \quad (4)$$

t_1, t_2, r_1, r_2 are the transmission coefficients and reflection coefficients of the equivalent interfaces, respective-

ly. φ_1, φ_2 are the reflection phases of the equivalent interfaces and $\delta_0 = \frac{2\pi}{\lambda} nd$ is the propagation phase.

Let's simplify it further,

$$\overline{R} = \sqrt{R_1 R_2},\ T_0 = \frac{T_1 T_2}{\left(1 - \overline{R}\right)^2},\ F = \frac{4\overline{R}}{\left(1 - \overline{R}\right)^2},$$

$$\theta = \frac{1}{2}\left(\varphi_1 + \varphi_2 - 2\delta\right) \quad , \quad (5)$$

$$T = \frac{T_0}{1 + F\sin^2\theta} \quad . \quad (6)$$

The position of the maximum transmittance, also the central wavelength, is determined by the following equation:

$$\theta = \frac{1}{2}\left(\varphi_1 + \varphi_2 - 2\delta_0\right) = -k\pi \quad , \quad (7)$$

$$\lambda = \frac{2nd}{k + \left[\left(\varphi_1 + \varphi_2\right)/2\pi\right]} \quad , \quad (8)$$

φ_1 and φ_2 are the reflection phases of the top and bottom equivalent interfaces. So according to Eq. (8), when the embedded material remains unchanged, the resonant wavelength is related to the reflection phase of the top and bottom equivalent interfaces.

For the reflection phase of the top interface, it can be calculated according to TMM as follows. [18,19]

Supposing that the top DBR and the top cavity layer compose a j-th layer film, the admittance of the lower surface of the top equivalent interface can be written as follows according to the boundary conditions of plane electromagnetic wave propagation at the interface,

$$\begin{bmatrix} E_0 \\ H_0 \end{bmatrix} = \left\{ \prod_{j=1}^{K} \begin{bmatrix} \cos\delta_j & \frac{i}{\eta_j}\sin\delta_j \\ i\eta_j \sin\delta_j & \cos\delta_j \end{bmatrix} \right\} \begin{bmatrix} E_{K+1} \\ H_{K+1} \end{bmatrix}, \quad (9)$$

E_0 and H_0 are the amplitudes of the electric and magnetic fields of the incident wave, respectively. δ_j is the phase thickness of the film layer. η_j is the admittance of the j-th layer film and K is the number of films. There are only forward waves and no backward waves, corresponding to $H_{K+1}/E_{K+1}=\eta_{K+1}$. So,

$$\begin{bmatrix} E_0 \\ H_0 \end{bmatrix} = \left\{ \prod_{j=1}^{K} \begin{bmatrix} \cos\delta_j & \frac{i}{\eta_j}\sin\delta_j \\ i\eta_j \sin\delta_j & \cos\delta_j \end{bmatrix} \right\} \begin{bmatrix} 1 \\ \eta_{K+1} \end{bmatrix} E_{K+1} . \quad (10)$$

Let $B=E_0/E_{K+1}$ and $C=H_0/E_{K+1}$ represent the normalized electric and magnetic fields of the equivalent interface, then one can get:

$$\begin{bmatrix} B \\ C \end{bmatrix} = \left\{ \prod_{j=1}^{K} \begin{bmatrix} \cos\delta_j & \frac{i}{\eta_j}\sin\delta_j \\ i\eta_j \sin\delta_j & \cos\delta_j \end{bmatrix} \right\} \begin{bmatrix} 1 \\ \eta_{K+1} \end{bmatrix}. \quad (11)$$

For p- polarized waves and s- polarized waves, the phase thickness of the film layer is

$$\delta_j = \frac{2\pi}{\lambda} n_j d_j \cos\theta_j \quad , \quad (12)$$

the angle of refraction θ_j is determined by the refraction theorem. n_j and d_j are the refractive index and physical thickness of the j-th layer film, respectively. η_0 is the admittance of the incident medium, which is considered a positive real number. Then there is

$$\varphi = arc\tan\left(\frac{i\eta_0\left(CB^* - BC^*\right)}{\eta_0^2 BB^* - CC^*}\right) \quad , \quad (13)$$

φ_1 and φ_2 of Eq. (8) can be expressed by Eq. (13). Therefore, when we change the embedded position, the thickness of the first layer of the equivalent interface is changed, which in turn changes the reflection phase according to Eq. (13). And then according to Eq. (8), the reflection phases of the top and bottom equivalent interfaces change as the resonant wavelength changes.

2 Results and discussion

2.1 The effect of embedded position on the resonant mode

The transmission spectra of embedded material at different positions are studied first. In this part, the only variable is the position of the embedded material. Other parameters such as the number of DBR pairs, embedded material thickness and cavity layer thickness are fixed. The specific structure is $(LH)^6\ x\mathrm{L}\ \mathrm{E}\ (8\text{-}x)\mathrm{L}\ (HL)^6$. The total thickness of the cavity layer is 8L and the thickness of E is 50 nm. Figure 2 (a) shows the transmissivity spectra when they are located in different positions. The resonant mode keeps the same when the position of embedded material is in the even (or odd) cavity layer (x is an even or odd number) as shown in Fig. 2(a). This is because the 2L is the period of the changed cavity layer. The reflection phase difference of the equivalent interface is 2π, so the resonant mode does not change either. However, the resonant mode changes periodically with positions. The resonant wavelength is minimum when embedded in the position of an even cavity layer, and redshifts to the maximum when embedded in the position of an odd cavity layer. Therefore, there is a maximum peak shift (MPS) when embedded in a 2D material and the resonant wavelength is the smallest when embedded in an even cavity layer, and redshift occurs when embedded in other positions. This is caused by the reflection phase variation and the phase difference between the even and the odd layer is π. Figure 2 (b) shows the change rule of the resonant mode from the odd layer to the even layer. We can find that the redshift of the resonant mode displays gradually as the embedded position increases. When the embedded position is in an odd number layers, the MPS occurs. Although the total physical thickness of the cavity layer is constant, the resonant peak periodically shifts as the same material is embedded in different positions. This represents that the strongest coupling position has changed because of the different embedded positions. Therefore, the electric field distribution along the direction of incidence is calculated at different positions as shown in Fig. (3).

Figure 3 (a) shows the distribution of the electric field in the F-P cavity without the embedded material at the designed wavelength, which is a typical standing

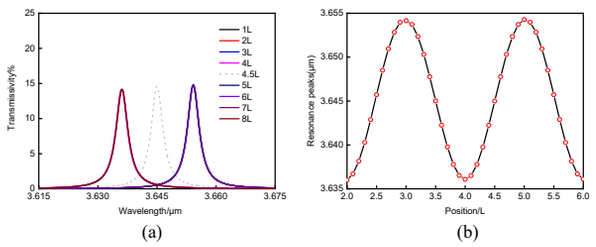

Fig. 2 (a) The transmission spectra of embedded materials with the same thickness (50 nm) at different locations, (b) the variations of resonant modes with the same thickness (50 nm) at different embedded locations
图2 (a) 相同厚度(50 nm)的嵌埋材料在不同嵌埋位置的透射谱,(b) 相同厚度(50 nm)的嵌埋材料在不同嵌埋位置的共振模式的变化

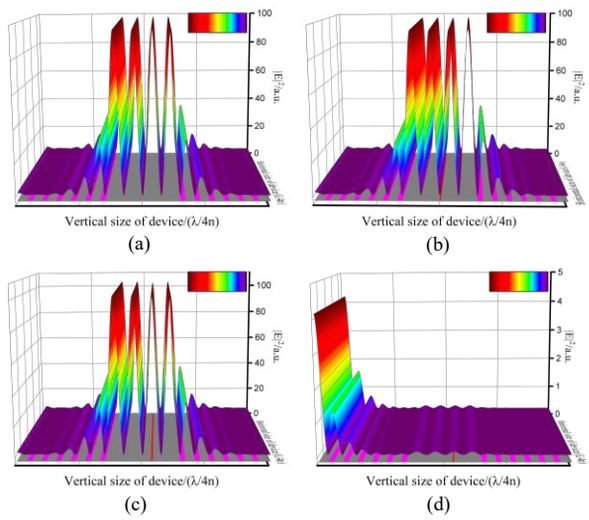

Fig. 3 (a) The electric field distribution without embedding (λ = 3.6 μm), (b) the electric field distribution embedded in 4L (λ = 3.64 μm), (c) the electric field distribution embedded in 3L (λ = 3.65 μm), (d) the electric field distribution embedded in 3L (λ = 3.6 μm)
图3 (a) 没有嵌埋时电场分布 (λ = 3.6 μm),(b) 材料嵌埋在4L处的电场分布 (λ = 3.64 μm),(c) 材料嵌埋在3L处的电场分布 (λ = 3.65 μm),(d) 材料嵌埋在3L处的电场分布 (λ = 3.6 μm)

wave mode. There are four positions with the strongest electric field intensity in the cavity layer with a cavity of 8L. If the embedded material is very thin, much less than the cavity layer thickness, the choice of the embedded location is very important. Figures 3(b) and 3(c) are the distributions of the electric fields in the cavity when the same thickness of material is embedded in an even and an odd layer at the resonant wavelength, respectively. In Fig. 3(b), we can see that the embedded material is placed in an even layer with the minimum electric field, which is the worst position for the light-matter interaction. On the contrary, when the gain material is embedded in an odd layer, the coupled electric field is the strongest at the resonant wavelength of 3.65 μm, which is the best position for the light-matter interaction. Figure 3(d) is the distribution of electric field in the DBR cavity when the material embedded in an odd layer at the designed wavelength of 3.6 μm, whose intensity is low. This result shows that the cavity has a good ability to localize light at the resonant wavelength. According to the above four kinds of electric field distribution, as shown in Fig. 3, we can see that the basic mode in the cavity does not change, but the resonant mode varies when the material is embedded in different positions. Therefore, we can speculate the embedded position of the material and calculate the coupling efficiency based on the electric field at a location after testing the transmission spectrum. It is necessary to study the interaction between light and matter. At the same time, we can design the embedded position to tune the resonant wavelength. This is a simple and efficient way to fabricate integrated optical devices. Therefore, we can choose to embed 2D materials in the position with the strongest coupling to enhance the interaction between light and matter or embed materials in the weakest position to reduce the absorption loss and lower the threshold power of devices in practical applications.

2.2 The effect of the number of DBR pairs on the resonant mode

The number of DBR pairs is a key parameter for DBR performance, therefore we discuss the changes of the resonant mode under different DBR pairs as shown in Fig. 4. In this part, the variable is mainly the number of DBR pairs which is considered under two extreme positions. Other parameters such as the embedded material thickness and the cavity layer thickness are fixed. The specific structure is $(LH)^m$ *x*L E (8-*x*) L $(HL)^m$. The total thickness of the cavity layer is 8L and the thickness of E is 50 nm. The resonant modes of odd and even layers do not change as shown in Fig. 4. When the DBR pairs vary from 4 to 8 pairs, which means the number of DBR pairs has little to do with changing the resonant mode. For each LH stack that is propagated by light, the reflection phase changes by 2π. So, the resonant wavelength will not change according to Eq. (8). However, the transmissivity decreases gradually with the increase of the DBR pair number. The full width at half maximum (FWHM) of resonant peak also decreases with the increase of the DBR pair number, while the quality factor increases correspondingly. Although these two parameters have no effect on the resonant mode, they still mutually restrict the quality of the cavity, which should be considered in the process of light-matter interaction.

2.3 The effect of the cavity layer thickness on the resonant mode

The cavity layer thickness is important to the localization of the electric field and the resonant mode can be changed by tuning the cavity layer thickness. In this part, the influence of the cavity layer thickness on the resonant mode under two extreme positions is investigated. Other parameters such as the embedded material thickness and the number of DBR pairs are fixed. The specific structure is $(LH)^6$ *x*L E *y* L $(HL)^6$. The number of DBR pairs is set as 6 and the thickness of E is 50 nm. The cavity layer thickness is changed from 2 to 8 ($x + y$ =

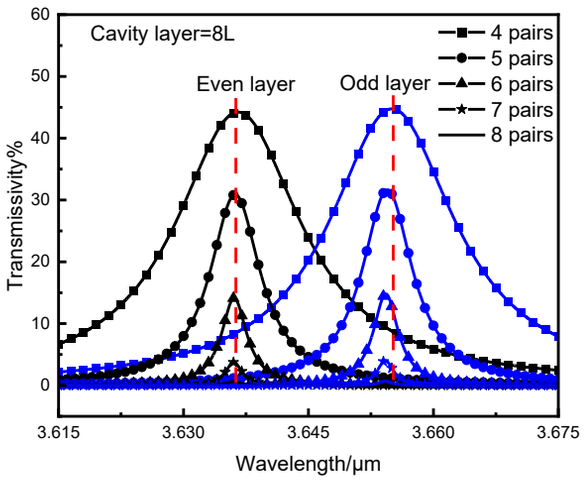

Fig. 4 Transmission spectra of the cavity under different numbers of DBRs with the cavity layer thickness 8L and the embedded material thickness 50 nm
图4 在腔长厚度为8L以及嵌埋材料厚度50 nm时不同DBR对数下腔的透射谱

2, 4, 6, 8). The MPS is calculated as shown in Fig. 5 (a). We can see that the MPS becomes smaller with the increase of the cavity layer thickness as shown in Fig. 5 (b). The propagated phase is smaller when the cavity layer thickness is thinner according to Eq. (12). The maximum shifts and the cavity layer thickness are fitted using an inversely proportional relationship, which is consistent with Eq. (8). Therefore, the resonant peak can be selected by adjusting the cavity layer thickness. Given the effect of the embedded position on the resonant mode, the strongest coupling of the selected resonant mode can be achieved by tuning these two factors.

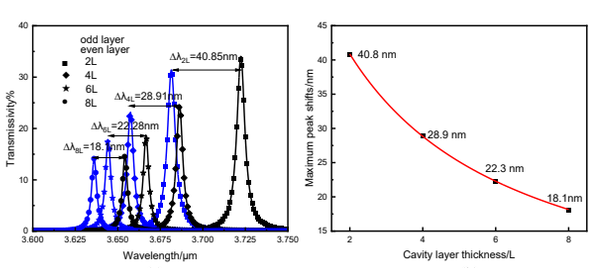

Fig. 5 (a) The cavity transmissivity with different cavity thicknesses, (b) the maximum peak shifts vary with different cavity thicknesses
图5 (a) 不同腔层厚度条件下腔的透过率,(b) 不同腔层厚度下的最大峰位移变化

2.4 The effect of the embedded material thickness on the resonant mode

The influence of the embedded material thickness is also important on the resonant mode. Therefore, it is studied theoretically since single or low layer material is very difficult to be controlled freely in experiments. The variable here is mainly the embedded material thickness under two extreme embedded positions. Other parameters such as the cavity layer thickness and the number of DBR pairs are fixed. The specific structure is $(LH)^6\ xL\ E\ (8\text{-}x)\ L\ (HL)^6$. We find that there is a linear relationship between the MPS of cavity mode and the thickness of embedded material in a limited thickness range, as shown in Fig. 6. The resonant mode mainly changes with the embedded material thickness by tuning the propagation phase, similar to the cavity layer thickness. Therefore, such a property can be used to select the modes that can be coupled precisely for coupling by changing the embedded material thickness.

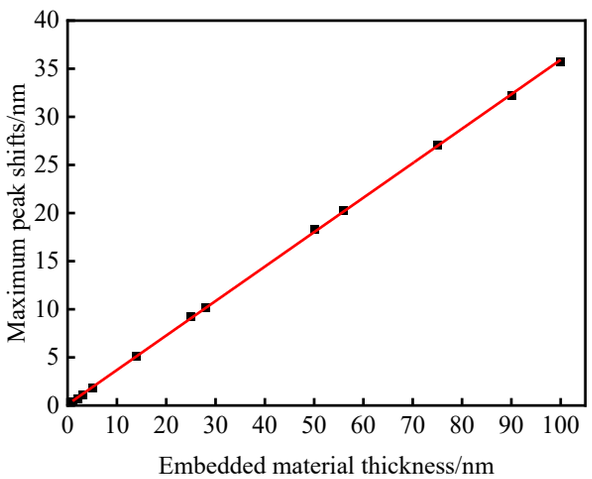

Fig. 6 The MPS of the cavity mode varies with the thickness of the embedded material
图6 最大偏移量随嵌埋材料厚度的变化

3 Conclusions

In summary, the effects of the embedded materials on the cavity resonant mode in DBR cavities have been studied intensively. The embedded position, number of DBRs pairs, cavity layer thickness and embedded material thickness are four key parameters that affect the resonant mode selection and coupled electric field distribution. The cavity resonant mode changes periodically with the embedded positions with a change period of 2L. Therefore, there is an MPS with a period that decreases with the increase of the cavity layer thickness. It is also proportional to the embedded material thickness when it is thin. One can control the material embedded in different positions of the cavity or the cavity layer thickness to tune the resonant wavelength and achieve the strongest light-matter interaction. Although the number of DBR pairs does not affect the resonant mode, it still plays an important role in the localization of the light field. These results provide guidance for precise optical devices and analysis of experimental phenomena, which can be applied to different wavelength ranges of DBR cavity structures.

References

[1] Xiong X, Xiao Y-F. Hybrid plasmonic-photonic microcavity for enhanced light-matter interaction [J]. *Science Bulletin*, 2022, **67** (12): 1205-8.

[2] Zhang Q, Wang S-W, Liu X, *et al*. Low threshold, single-mode laser based on individual CdS nanoribbons in dielectric DBR microcavity [J]. *Nano Energy*, 2016, **30**: 481-7.
[3] Shang J, Cong C, Wang Z, *et al*. Room-temperature 2D semiconductor activated vertical-cavity surface-emitting lasers [J]. *Nat Commun*, 2017, **8**(1): 543.
[4] Wang S, Xia C, Chen X, *et al*. Concept of a high-resolution miniature spectrometer using an integrated filter array [J]. *Opt Lett*, 2007, **32**(632-634).
[5] Xuan Z, Liu Q, Cui Z, *et al*. On-chip short-wave infrared multispectral detector based on integrated Fabry - Perot microcavities array [J]. *Chinese Optics Letters*, 2022, **20**(6): 061302.
[6] Xuan Z, Li J, Liu Q, *et al*. Artificial Structural Colors and Applications [J]. *Innovation (Camb)*, 2021, **2**(1): 100081.
[7] Vahala K J. Optical microcavities [J]. *Nature*, 2003, **424**: 8.
[8] Pei S-H, Song Z-X, Lin X, *et al*. Interaction between light and single quantum-emitter in open Fabry-Perot microcavity [J]. *Acta Physica Sinica*, 2022, **71**(6): 060201.
[9] Won R. Two-dimensional material nanophotonics [J]. *Nature Photonics*, 2010, **4**(12): 882.
[10] Wu S, Buckley S, Schaibley J R, *et al*. Monolayer semiconductor nanocavity lasers with ultralow thresholds [J]. *Nature*, 2015, **520**(7545): 69-72.
[11] Wang Z, Wang P, Wang F, *et al*. A Noble Metal Dichalcogenide for High-Performance Field-Effect Transistors and Broadband Photodetectors [J]. *Advanced Functional Materials*, 2019, **30**(5): 1907945.
[12] Peng M, Yu Y, Wang Z, *et al*. Room-Temperature Blackbody-Sensitive and Fast Infrared Photodetectors Based on 2D Tellurium/Graphene Van der Waals Heterojunction [J]. *ACS Photonics*, 2022, **9**(5): 1775-82.
[13] Hu W, Ye Z, Liao L, et al. 128×128 long-wavelength/mid-wavelength two-color HgCdTe infrared focal plane array detector with ultralow spectral cross talk [J]. *Opt Lett*, 2014, **39**(17): 5130-5133.
[14] Hu W, Chen X, Ye Z, et al. A hybrid surface passivation on HgCdTe long wave infrared detector with in-situ CdTe deposition and high-density Hydrogen plasma modification [J]. *Appl Phys Lett*, 2011, **99**(9): 091101.
[15] Zhang Y, Wang S, Chen S, *et al*. Wavelength-Tunable Mid-Infrared Lasing from Black Phosphorus Nanosheets [J]. *Adv Mater*, 2020, **32**(17): e1808319.
[16] Zhao X, Yan Y, Cui Z, *et al*. Realization of strong coupling between 2D excitons and cavity photons at room temperature [J]. *Opt Lett*, 2020, **45**(24): 6571-4.
[17] Xie M, Wu Z, Cui H, *et al*. On-site determination of optical constants for thin films [J]. *Journal of Infrared and Millimeter Waves*, 2022, **41**(5), 888-893.
[18] Liu Q, Zhao X, Li C, *et al*. Coupled Tamm plasmon polaritons induced narrow bandpass filter with ultra-wide stopband [J]. *Nano Research*, 2022, **15**(5): 4563-8.
[19] Cui Z, Yan Y, Liu Q, *et al*. Accurate determination of low-dimensional materials' complex refractive index by cavity resonant method [J]. *Optical Materials*, 2022, **131**: 112682.